energies

MDPI

Article

Seamless Integration of an Autonomous Induction Generator System into an Inverter-Based Microgrid

Catalin Petrea Ion * and Ioan Serban

Department of Electrical Engineering and Applied Physics, Transilvania University of Brasov, 29 Eroilor, 500036 Brasov, Romania; ioan.serban@unitbv.ro

* Correspondence: catalin.ion@unitbv.ro; Tel.: +40-268-474-718

Received: 28 December 2018; Accepted: 14 February 2019; Published: 16 February 2019

Abstract: A control strategy for an autonomous induction generator (IG) system synchronization and seamless transfer to an inverter-based microgrid (MG) is presented in the current paper. The IG system control in autonomous mode is performed by a combination between a Voltage Source Inverter (VSI) and a Dump Load (DL). The MG consists of an MG leading inverter having on its DC side a supercapacitor-based energy storage system, two MG supporting inverters, and local loads. The paper presents the IG control part for the VSI-DL system, as well as the synchronisation algorithm that enables the smooth interconnection with the MG. An analysis of the IG impact on an islanded MG is also provided. Experimental validations accomplished on a complex laboratory test-bench have focused on the dynamic events associated with the IG system connection/disconnection to/from the MG and also on the MG response to a load being turned on and off when the IG operates connected to the MG. The obtained results have shown that the proposed synchronization algorithm ensures a seamless transfer for the IG system from autonomous to MG connected mode and vice-versa. Moreover, when a significant load transient occurs within the MG operation, the IG presence does not alter the MG stability.

Keywords: renewable energy; microgrid; induction generator; synchronization; transfer

1. Introduction

The renewable energy sources (RES) play a major role in electricity generation nowadays, operating along with energy storage systems (ESS) in autonomous microgrids (MGs) or as distributed generators (DGs) connected to the grid. For the first situation, optimal scheduling can lead to minimum operating costs [1], while in case of the second scenario, an optimized hierarchical control deals with adverse grid conditions [2]. A significant part of the available literature focuses on the MGs seamless transfer from autonomous to grid-connected mode and vice-versa. Within this topic, the synchronization algorithms embedded in the control structure of the power converters that interface an MG or an RES-based DG with the main grid have been extensively analysed [3,4], relying mainly on Phase Locked Loop (PLL) methods. An extensive review on the existing literature regarding the synchronization methods is provided in [3]. The study concluded that, even though new methods have been developed to overcome the drawbacks of classical PLLs, the latter ones are still extensively used because of their simplicity. Moreover, many adjustments have been made to PLLs to improve their performance when dealing with a weak grid. Reference [4] provides a comprehensive review of the new techniques for enabling the synchronisation of inverter units. They are compared based on their frequency adaptability, possibility of active and reactive power control, harmonic information, and design complexity.

In many situations, the synchronization part is treated in close relation with other features related to the power converters control/MG control hierarchy. For example, Reference [5] proposes a new

distributed active synchronization strategy that takes into account the harmonic components, for an MG reconnection to the grid under distorted and unbalanced voltage conditions. The synchronization part is included in the secondary MG control level, ensuring the reduction of the inrush current during grid reconnection. Reference [6] relies on the alternating direction method of multipliers to tackle the synchronisation phenomenon in inverter-based microgrids. The main advantage of using such a method is that it is not influenced by noise, being successfully tested on a modified 34-bus IEEE feeder system. Reference [7] investigates a multi-bus microgrid having a control system that generates, besides two synchronisation correction signals (for voltage and frequency), a distributed frequency and phase synchronisation among the adjacent DG units. A single DG unit with a dual-converter system and a single controller, combining both voltage control (VCM) and current control methods (CCM) is presented in [8]. For seamless transfer from grid-tied mode to islanding operation the controller uses the VCM option. Reference [9] proposes an adaptive total sliding-mode control applied to a grid-connected single-phase inverter which, depending on the grid availability, consists in two algorithms, one for grid-connected mode and another for stand-alone operation. Both algorithms ensure stable operation and seamless transfer between the two operating modes. The authors of [10] use a voltage source converter (VSC)-based synchronizer to implement a PLL-based active synchronization method. By addressing the whole process as a PLL design issue, the proposed active synchronizer is said to help reduce the synchronization time by an order of magnitude. A more particular situation is presented in [11], where the synchronization of an active load with an inverter-based microgrid without the use of a PLL is investigated. The synchronization algorithm relies in brief on creating a reference frame for the active load and then referring the active load voltages and currents to the newly created reference frame.

The power produced by generating units based on RES such as wind and solar is subject to several transformation stages before being delivered to the MG loads/grid, the last stage being ensured by inverters. Nevertheless, mainly in case of micro hydro units operating at fix speed, a squirrel cage induction generator (IG) is responsible for directly providing power to the consumers. In autonomous mode, at least one power converter is required for voltage and frequency balancing; in addition, a capacitor bank for self-excitation is included. Thus, in the point of common coupling (PCC) of such isolated systems are connected the generator, the power converter, the capacitor bank and the local loads. Extensive research has been done to study the autonomous behaviour of such a system, more recent solutions relying, for instance on a Distribution Static Compensator for voltage regulation and power quality enhancement [12], or on a Generalized Impedance Controller to ensure, besides voltage and frequency regulation, balanced stator currents in case of unbalanced loads [13].

The squirrel-cage IG synchronization with the grid is much simpler than in the case of synchronous generators, as the main condition is to bring the machine at its synchronous speed before closing the grid switch. The major drawback is the need for reactive power for generator magnetization which leads to high inrush currents. A feeder simulator was developed in [14] in order to assess the IG influence on the PCC in case of grid connection, loading and disconnection. To decrease the inrush current specific to the grid connection process, a system consisting of a power electronic converter plus a controllable load was investigated in [15], while in Reference [16] a thyristor-based Soft-starter was employed. A three-phase IG can also be connected to a single-phase grid through an uncontrolled bridge rectifier plus a single-phase inverter [17].

Regarding autonomous MGs interaction with the grid, the literature is comprehensive, a particular category being inertia-less MGs [18,19]. But in which concerns the case of autonomous IG systems the literature lacks studies regarding their synchronization with the grid and even less with an MG. For example, the authors of [20] investigate a wind-solar-diesel MG in which the IG is powered by a diesel engine (DE) and can operate in parallel with a permanent magnet brushless DC generator driven by a small wind turbine and a PV array, the control being performed by a VSC in combination with a battery storage system. The MG can be connected to the grid, thus enabling bidirectional power flow, but in this case, the IG-DE unit is disconnected; it only synchronizes with the MG when the

latter operates in autonomous mode and the available renewable energy cannot sustain the local loads. Another similar approach is presented in [21], case in which a wind-driven IG, controlled by an active voltage and frequency regulator (actually a voltage source inverter (VSI) with a controllable resistor on the DC link), is investigated when being paralleled/disconnected with/from the power grid.

The present paper tackles a very particular situation, in which an autonomous IG system is connected/disconnected to/from an inverter-based microgrid. Also, when operating in parallel with the considered MG, the IG influence during an MG load variation is investigated. After the introduction, the paper is organized as follows: Section 2 details the system configuration and the IG control, an analysis of the IG impact on an islanded MG is provided in Section 3, Section 4 shows the experimental results while Section 5 presents the main paper conclusions.

2. System Configuration and Control

The IG system is connected to a three-phase MG, which includes several inverter-based DGs and energy storage systems ESS. The general topology of the MG is represented in Figure 1, where an MG leading inverter (MGLI) coordinates the MG operation both in islanded and in grid-connected mode. As shown in Figure 1, besides the power line that interconnects all MG sources, a communication bus is included to transfer data between the MGLI and each unit that participate in the MG control mechanism. Moreover, the proposed MG allows a straightforward way to integrate it with the utility's control level by means of a communication channel between MGLI and a distribution system operator (DSO). A comprehensive description of the MG solution is provided in [22,23], while this paper goes further and analyses the impact an IG has on the MG operation. Therefore, being outside the scope of the current paper, the specific control mechanisms of the MG will not be discussed.

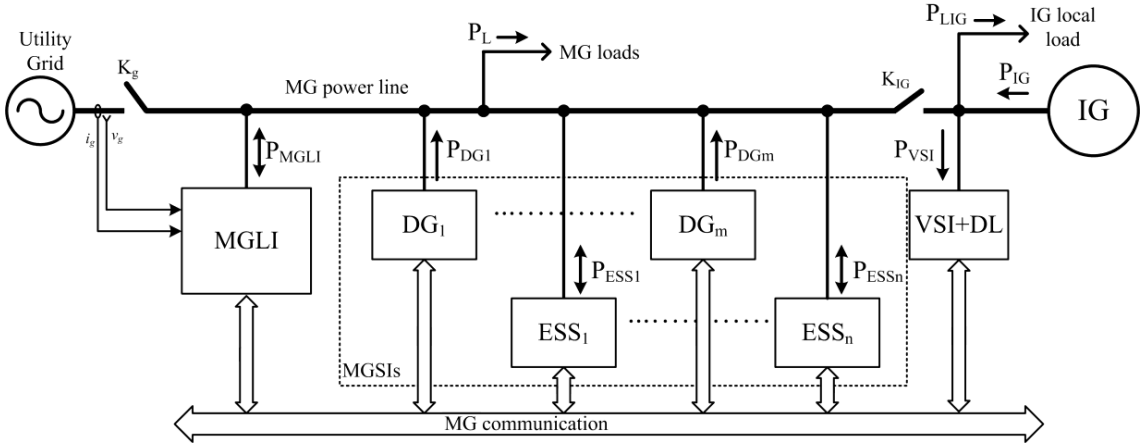

Figure 1. General topology of the microgrid (MG) with an integrated induction generator (IG) system.

In the proposed scheme, the IG can operate by itself supplying the local load, and it can seamlessly connect to the MG when necessary. By this approach, the IG forms a separate section of the MG, separated by the main grid through the IG relay K_G, controlled by the IG control system as described in Section 2.2. The concept of sectionalizing MGs has been previously discussed in the literature [24,25] and it has shown that, although the complexity of the system increases, the system's reliability and security of supply can be greatly improved. Moreover, the direct connection of the IG provides a natural inertia to the system, which is exploited here to increase the stability of the MG dominated by inverter-based sources.

2.1. IG System Configuration

The IG system consists in a squirrel-cage induction generator driven by a hydraulic turbine emulator, a capacitor bank (C_{exc}) for generator excitation and local loads, as shown in Figure 2. The K_G switch ensures the connection to the inverter-based MG. The voltage and frequency are controlled

by a VSI interfaced through a high-voltage DC link (C_{dc}) with a Dump Load (DL) circuit. The VSI connection to the AC bus is ensured by an LC filter. The control strategy has some particular aspects, as an uncontrolled micro hydro turbine is emulated; by considering constant the output power of the IG, the DL role is to dissipate the difference between the power produced by the IG and the one absorbed by the local loads. Moreover, excepting the IG start-up process, during which a controlled driving algorithm is implemented [26], the VSI operates with a fixed frequency reference. To improve the IG system behaviour during intense dynamic events, a Super Capacitor Storage System can be included within the VSI DC-link through a bidirectional DC-DC converter, as detailed in [27].

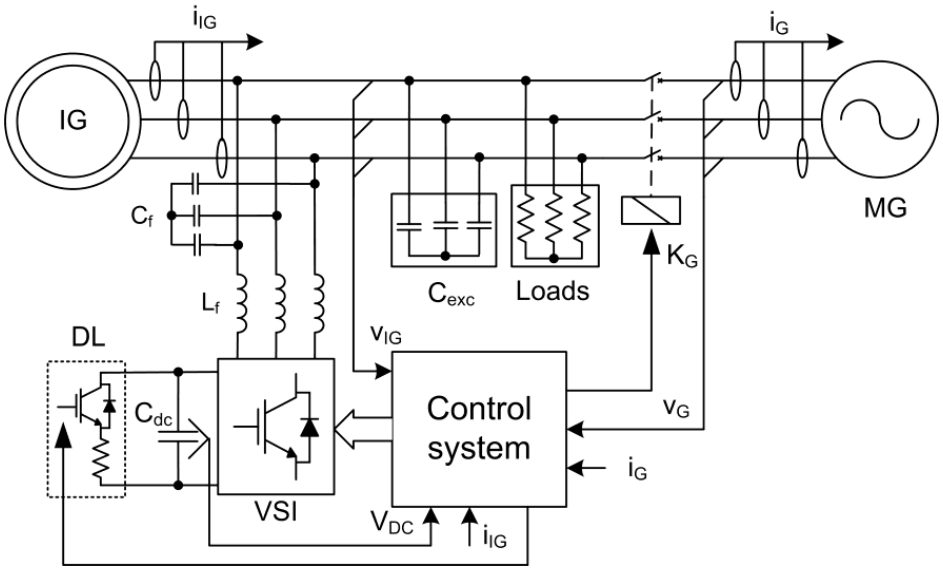

Figure 2. IG system configuration.

2.2. The IG System Control

The IG system control structure is presented in Figure 3. It consists in three loops responsible for providing (from top to bottom): the synchronisation signal for the K_G switch, the 6 pulse-width-modulation (PWM) pulses for the VSI and the DL PWM signal respectively.

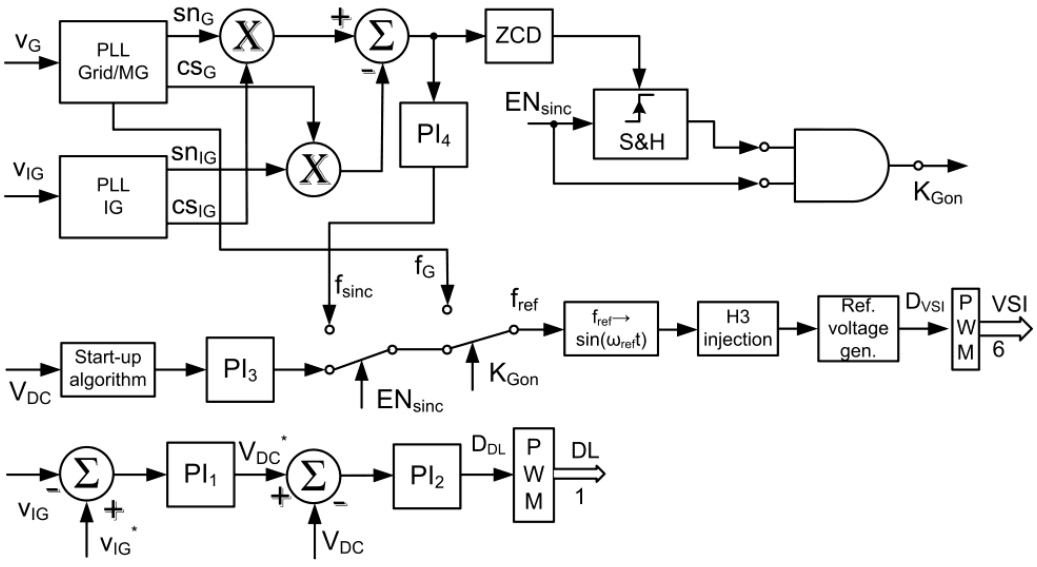

Figure 3. Block diagram of the IG system control.

The DL control loop relies on two proportional-integrative (PI) regulators, the first one (PI_1) being used to compensate for the possible voltage drops. It generates the DC voltage reference signal (V_{DC}*) for the second regulator (PI_2) that continuously adjusts the PWM duty cycle of the DL transistor to keep the DC voltage constant (V_{DC}).

The VSI control loop generates the PWM pulses for the inverter bridge transistors. Having as input the V_{DC} voltage (since it also has to initialize the start-up process with the help of a DC source connected in the DC link), by means of a third PI regulator (PI_3) the start-up algorithm provides a ramp reference frequency, which, after the IG voltage reaches the rated value, is set to 50Hz for autonomous operation.

In order to synchronize the IG system with the inverter-based MG, the control system uses two PLLs, one for IG system voltage and another for the MG voltage, having an internal structure as in [28]. The two PLLs provide the estimation of the phases of the two voltages in terms of their sine and cosine (sn_{IG}, cs_{IG}/sn_G, cs_G). As an additional signal, the MG PLL provides the frequency (f_G), which is used as reference after the synchronisation process has been finished. Based on the difference between the phases of the two voltages, another PI regulator (PI_4) provides the synchronisation frequency (f_{sinc}) signal, and ensures that the VSI voltage to be in phase with the MG's one, while having similar frequencies.

The synchronization process is initiated by providing the EN_{sinc} signal which changes the VSI reference frequency from the fixed 50Hz value to f_{sinc}. When the IG voltage phase matches the MG voltage phase, a zero-crossing detector provides the trigger signal for a sample&hold (S&H) block, which gives the ON signal for the K_G switch. An AND logical operator is added to prevent the K_G switch closing if the EN_{sinc} signal has not been transmitted. The K_G ON signal is also used to modify the VSI reference frequency from f_{sinc} to f_G. After the synchronisation process is accomplished, the VSI control is disabled, being automatically re-initialized if an unplanned disconnection from the MG occurs.

3. Analysis of the IG Impact on an Islanded MG

The MG, with or without the IG section connected, can operate in two operating modes, namely islanded and grid-connected. A seamless transition between the two states is ensured by the MGLI by means of a complex synchronization and disconnection algorithm as detailed in [22]. A grid relay (K_g) allows the MGLI to physically connect and disconnect the MG to and from the grid. An important point worth noting here is that, since all the processes required for MG transition and operation to the grid are carried out by the MGLI, the other sources supplying the MG do not change their operating modes, while the information exchanged through the communication line remains the same as in the islanded operation case. By this approach, the IG control remains the same regardless it operates connected to the MG or to the grid. Therefore, the control system described previously includes only two operating cases, namely autonomous mode when the IG supplies its section (i.e., K_G is open) and grid- or MG-connected mode.

Since during grid-connected mode, the MG frequency is fixed (and so the IG's one), the entire system can fairly be considered stable. The main concerns regarding system stability are in the islanded operation, when the IG—depending on its power relative to that of the MG—can have a certain impact on the MG dynamics. Therefore, this section provides in the following an analysis of how the MG dynamic behaviour changes with the IG integration.

3.1. System Modelling

The adopted approach is based on simplified models that consider only the dominant mechanisms in the power-sharing and frequency control of the MG. Therefore, without losing important information about system dynamics in the targeted frequency domain, a system order reduction has been applied taking into account only the dominant time constants. As part of the simplifying assumptions, the dynamics of current and voltage control loops of the inverters are neglected (their time constants are

much smaller than the one associated with the MG frequency control), and the system is considered stable at high frequencies associated with the inverters' inner current control; hence in the following analysis the dynamic of the inverters will be neglected. This also means that, for the purpose of the analysis presented in this paper, the control mechanisms of the voltage and frequency can fairly be considered decoupled.

3.1.1. MG Model

The MG operation principle follows the concept of virtual synchronous generator (VSG), which is known to be an optimal solution to improving the inertia in systems with large penetration of inverter-based generators. As detailed in [22], the MGLI implements an original VSG algorithm, which provides several advantages over traditional VSG solutions, whereas rest of the inverters includes inertia emulation control scheme. The overall effect is an increase in the total system inertia and an improvement of the MG stability.

The MG frequency control mechanism is divided in two stages, namely primary and secondary. The primary control is responsible for the actions required to limit the MG frequency deviation following a disturbance and the VSG response has a major influence within this first control level of the frequency. After the primary response has passed, the secondary control level slowly acts on the inverters setting points to restore the MG frequency to the rated value (i.e., 50 Hz). This process is coordinated by the MGLI shown in Figure 1, which sends correction signals to each inverter by means of the communication line. As revealed in [22], there are several parameters of the controllers involved in this process that influence the performance of the MG transitory response, and the values found as optimal are used in this paper too.

The VSG-based control approach of the MG is implemented in the MGLI, which changes the MG frequency according to the change of active power balance in the MG following the swing equation of a virtual mechanical system (in per unit form):

$$T_{mVSG} - T_{eVSG} = 2H_{VSG}\frac{d\omega_{VSG}}{dt} + D{\cdot}\Delta\omega_{VSG} \tag{1}$$

where: ω_{VSG} is the VSG speed (with Δ denoting the deviation from rated value); H_{VSG} is the virtual inertia; T_{mVSG} and T_{eVSG} represent the virtual mechanical and electrical torques, and D is a damping coefficient.

The MG frequency during dynamic events is mainly imposed by the MGLI response according to (1). However, the other inverters connected in the MG may also provide a certain level of frequency support and, therefore, the MG frequency response will depend on the composite response of all inverters in the MG. Following the approach described in [22], the so-called MG-supporting inverters (MGSI), which can be part of the DGs and ESSs represented in Figure 1, will react to the MG frequency change by modifying their output active power as follows:

$$P_{MGSI} = P^* + \left(\Delta\omega_g + \delta\omega_{g2}\right)K_{fs} + \frac{d\Delta\omega_g}{dt}K_{fd} \tag{2}$$

where: P^* is the reference power of the inverter; $\Delta\omega_g$ is the MG frequency deviation; $\delta\omega_{g2}$ is a frequency correction signal received from MGLI during secondary control, as previously described; K_{fs} and K_{fd} are the droop and the inertial response gains.

Therefore, when the IG is not connected, the MG frequency response will be provided only by the online inverters, based on (1) and (2). In order to analyse how the IG impacts the MG dynamic behaviour when it is part of the MG (i.e., K_G is switched on), an IG model is added to the overall MG model, as described in the following.

3.1.2. IG Model

The IG model is based on a reduced-order representation, based on the Kloss's formula that provides an approximation of an induction machine electromagnetic torque as a function of its slip s [29]:

$$T_e(s) = \frac{2T_{ek}}{\frac{s_k}{s} + \frac{s}{s_k}} \tag{3}$$

where: T_{ek} is the breakdown torque; s_k is the critical slip.

The IG slip depends of the grid/MG angular frequency (ω_g), rotor angular speed (ω_r) and pole pairs (P), as expressed in (4).

$$s = 1 - P\frac{\omega_r}{\omega_g} \tag{4}$$

As previously mentioned, in the considered application, the IG is driven by a micro hydro turbine (MHT), and, therefore, the mechanical torque can be expressed as follows:

$$T_m(\omega_r) = T_{m0} - K_{MHT}\omega_r \tag{5}$$

where: ω_r is the rotor speed (a direct connection between the IG and MHT is considered), T_{m0} is the MHT starting torque (i.e., at $\omega_r = 0$); K_{MHT} is the natural torque-speed control gain of the MHT.

The IG rotor speed (ω_r) is derived from the generator motion equation:

$$\omega_r = \frac{1}{J_r}\int (T_m - T_e)dt \tag{6}$$

where: J_r is the combined generator and MHT inertia coefficient.

Finally, neglecting the IG internal losses, the IG output power (P_{IG}) is calculated as,

$$P_{IG} = T_e \cdot \omega_r \tag{7}$$

3.2. Analysis

In order to analyse the system behaviour with the IG connected, a specific MG is modelled using as reference the configuration used for experiments. The MG consists of one MGLI and two other supporting inverters, each having a rated power of 5 kW. An IG with a rated output power of 3.1 kW and driven by an MHT emulator is added to the MG, as shown in Figure 6. The analysis presented in this section uses the same parameters with the ones of the experimental platform (detailed in Section 4).

During islanded operation, the MG frequency dynamic response depends to a large extent on the composite inertia of the interconnected generators. A high inertia constant provides a better stability margin and allows the MG to more safely ride through transients caused by important events like heavy load switching, or loss of important generation capacities. However, achieving a high inertia constant in MGs based on generators interfaced by inverters implies transient energy resources available. For this purpose, the MG used in this study includes a supercapacitor-based energy storage system, which is interfaced with the MG by the MGLI. As previously described, the MGLI uses a VSG-based algorithm to control the MG frequency and to provide a certain level of inertia. Therefore, the current analysis is focused on the impact the IG has on the MG frequency control process. When connected to the MG the IG can provide a certain level of support, which depends on the MG inertia and the dynamic behaviour of the IG-MHT assemble. For this purpose, the VSG inertia constant has been varied within a large interval, namely from an inertia-less MG with H_{VSG} very small to the nominal value of H_{VSG} considered in the experimental analysis.

Figure 4 shows how the IG can influence the MG frequency response for a 2kW load connection, with the MGLI emulating an inertia constant of H_{VSG} = 1 s and H_{VSG} = 10 s. Due to its natural inertia, the IG has a positive impact on the MG frequency response, the maximum frequency deviation being slightly reduced in both cases. As it can be seen, at low MG inertia (i.e., H_{VSG} = 1 s) the IG response

is more significant than in the second case with high MG inertia. Moreover, the IG support is more pronounced in the case of very low inertia, as shown in Figure 5. An important point worth noting is that, in the analysed case, only the natural IG response is exploited. However, further improvements are expected if the VSI integrated to control the IG during autonomous operation (i.e., K_G is opened) is used to boost the IG natural response (this subject is reserved for future research).

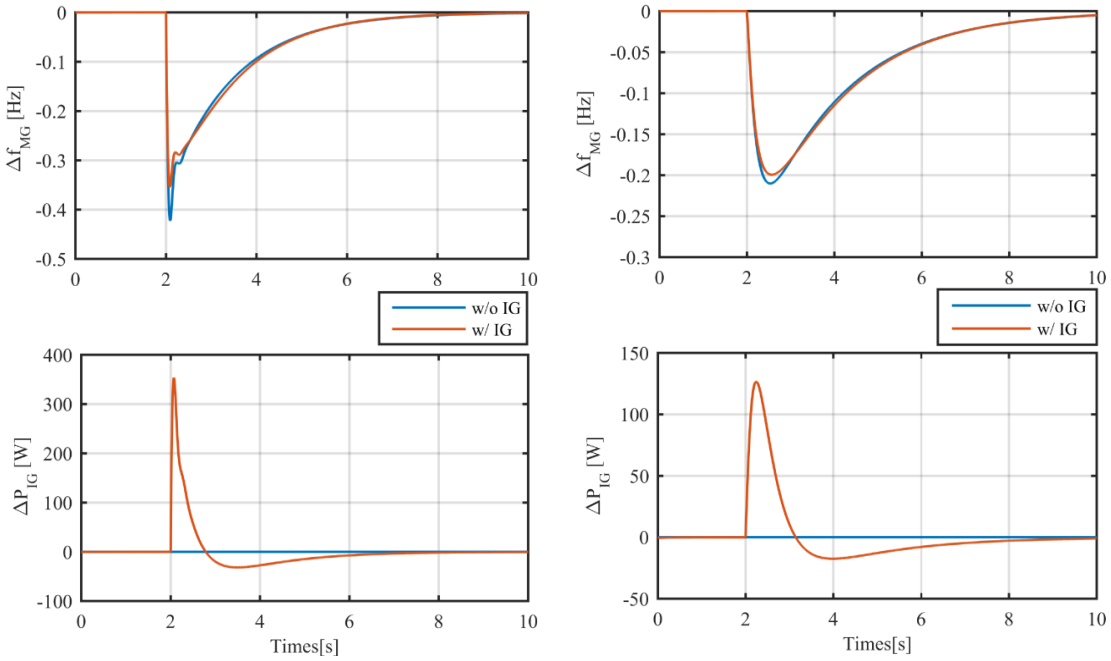

Figure 4. MG frequency deviation (Δf_{MG}) and IG output power deviation (ΔP_{IG}) for a 2 kW load connection, without and with IG connected: (**a**) H_{VSG} = 1 s; (**b**) H_{VSG} = 10 s.

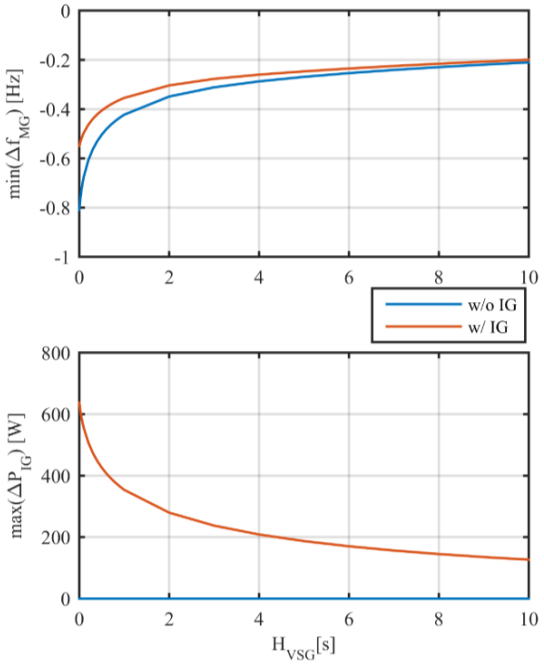

Figure 5. Variation with the MG inertia of the minimum MG frequency and the maximum IG power deviation for a 2 kW load connection.

4. Experimental determinations and discussion

According to the system structure presented in Figure 1, a complex laboratory MG prototype has been used to experimentally validate the proposed IG-based control solutions. The one-line diagram of the MG platform is represented in Figure 6a, which include three inverters (one MGLI and two MGSI) rated at 5 kW each, operating at a switching frequency of 10kHz and supplied with a DC-link voltage of V_{DC} = 650 V. The three-phase MG has a rated output voltage of 400 V and the rated frequency is 50 Hz. The MGLI includes on the DC-side a supercapacitor-based ESS, while the other two MGSI are supplied by a DC source. On the control side, each inverter is controlled independently by dSPACE DS1103 real-time boards. The MG communication shown in Figure 1 is implemented by means of a CAN network, which interconnects each dSPACE system.

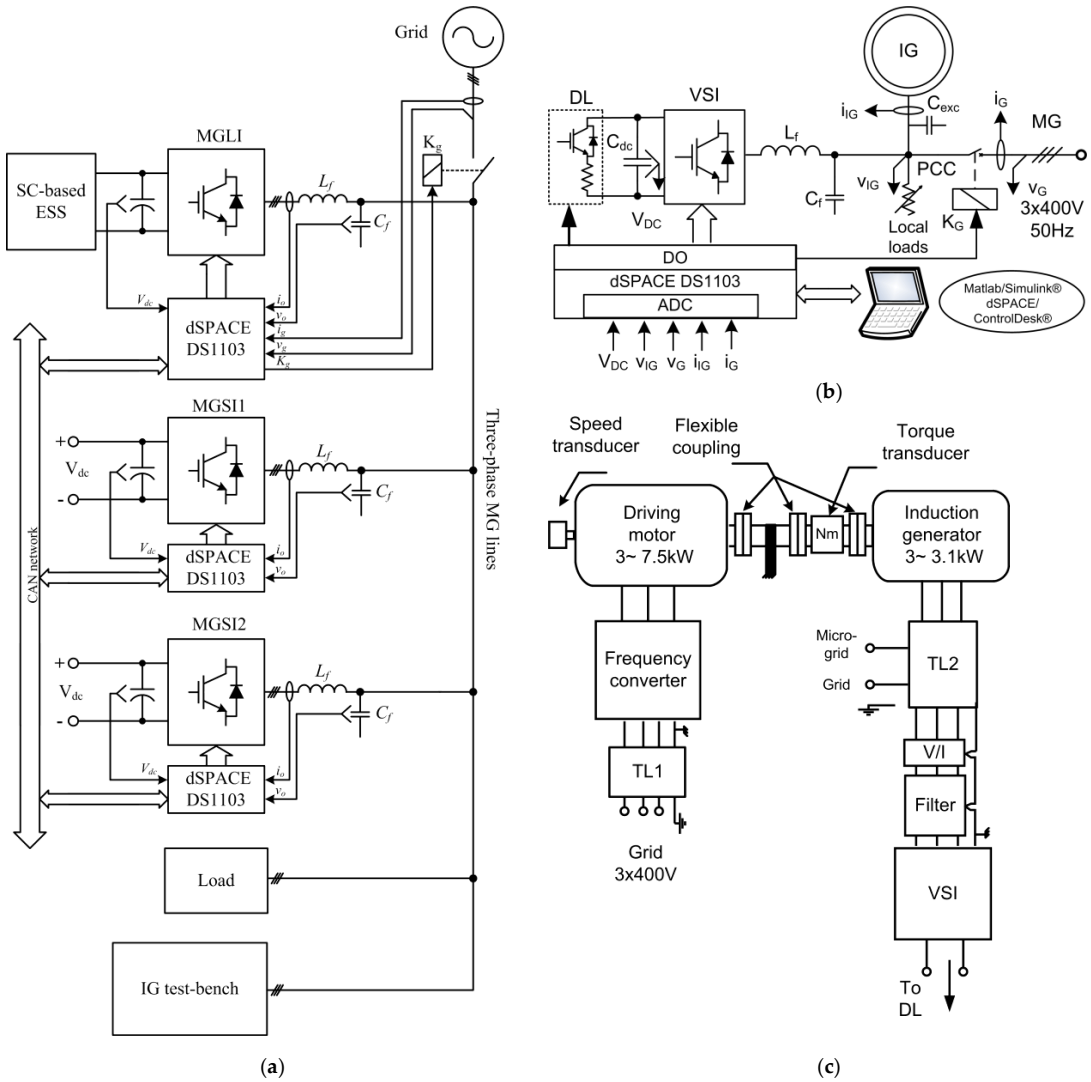

Figure 6. Experimental test-bench: (**a**) MG diagram with the integrated IG; (**b**) IG system electrical part, (**c**) IG system electro-mechanical part.

A specialized IG test-bench is added in parallel to the MG. The block diagram of the IG system is detailed in Figure 6b (electric side) and in Figure 6c (electro-mechanical side). The MHT is emulated by a 7.5 kW induction motor fed by a frequency converter, specially controlled to follow the mechanical characteristic of a micro-hydro turbine, as presented in [26]. A torque transducer is placed on the common shaft between the driving motor and the IG, a rotational speed transducer being also employed. An important aspect worth being mentioned is that, due to the limitations of the

experimental IG test-bench, the IG output power is limited to 2 kW. The detailed parameters for the IG system and MG are given in Appendix A.

To evaluate the integration of the IG system within an inverter-based MG, the experimental analysis focuses on the two cases of interest:

(Case 1) The synchronization of the autonomous IG system (controlled by the VSI-DL) with the MG;
(Case 2) The behaviour of the IG system, operating in parallel with the MG, during a significant load variation.

To assess the IG system behaviour during the above-mentioned situations, the parameters measured during the experimental tests were used to calculate the following performance indices, express by relations (8)–(11): voltage deviation (ΔV), frequency deviation (Δf), IG speed deviation (Δn) and IG active power deviation (ΔP_{IG}):

$$\Delta V[\%] = \left(1 - \frac{V_{MG}}{V_0}\right) \cdot 100 \tag{8}$$

$$\Delta f[\%] = \left(1 - \frac{f_G}{f_0}\right) \cdot 100 \tag{9}$$

$$\Delta n[\%] = \left(1 - \frac{n_{IG}}{n_0}\right) \cdot 100 \tag{10}$$

$$\Delta P_{IG}[\%] = \left(1 - \frac{P_{IG}}{P_{IG0}}\right) \cdot 100 \tag{11}$$

where: V_{MG} is the MG line-to-line voltage (V_0 = 400 V), f_G is the MG frequency (f_0 = 50 Hz), n_{IG} is the generator speed at 2 kW loading (n_0 = 1541 RPM) and P_{IG} is the generator power (P_{IG0} = 2 kW).

The results are synthesized in Table 1.

Table 1. Parameters evaluation.

	Event	ΔV [%]	Δf [%]	Δn [%]	ΔP_{IG} [%]
Case1	Connection to MG	5	0.84	0.53	23
	Disconnection from MG	5.73	0.5	0.27	16.2
Case2	MG load increase	3.96	0.7	0.39	17.9
	MG load decrease	3.42	0.8	0.32	22.6

The situation in which the IG system is connected to the inverter-based MG is investigated first. Thus, as the VSI receives the synchronization signal, it starts changing the frequency of its output voltage (V_{VSI}) in order to bring its voltage in phase with the MG one (V_{grid}), as in normal operation they are likely to be out of phase. When the two voltages do match, the signal for the K_G switch is activated, thus enabling a seamless transfer of the IG system from autonomous to MG connected mode, as shown in Figure 7. In the upper part of Figure 7 the VSI frequency variation is shown, while at the bottom are highlighted the phase of the two voltages when the synchronization process was enabled (left side), and during the K_G switch closing (right side).

Figure 8 highlights the IG system smooth transitions from autonomous to MG connected mode and vice-versa. For a better visualisation of the voltage variation during the transitory regime a zoom was provided for each of the two situations. As can be seen, the inherent disturbances are insignificant, which demonstrates the good performance of the proposed control solution.

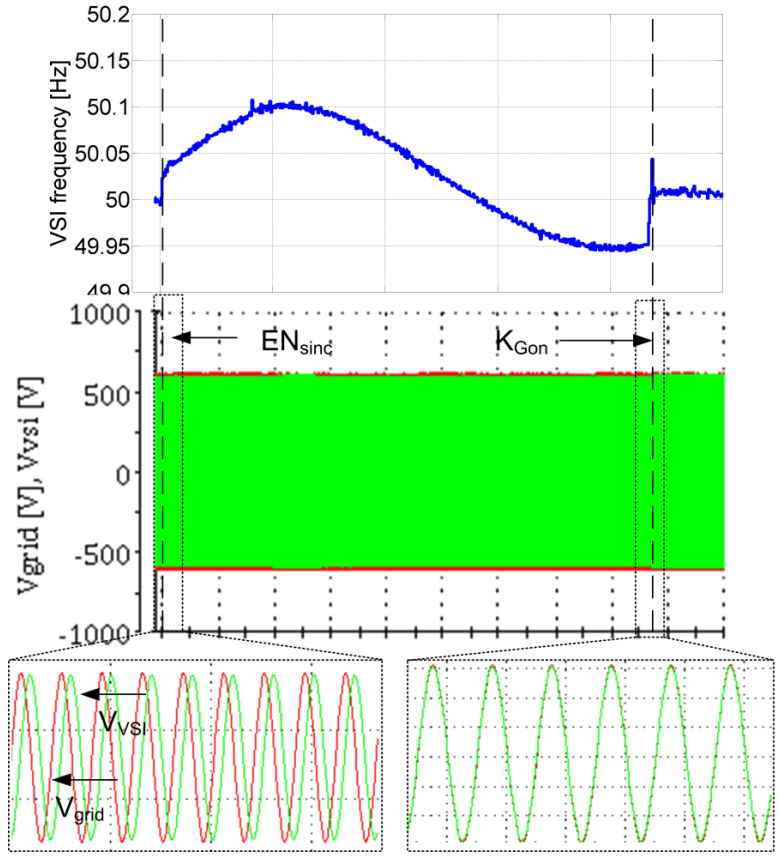

Figure 7. Synchronization process detailing.

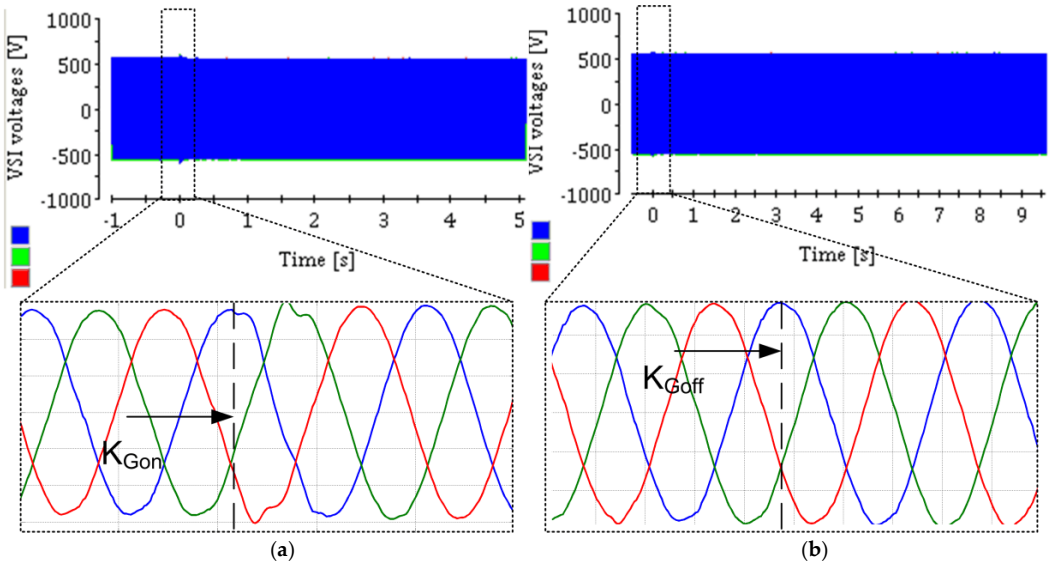

Figure 8. Transfer from autonomous to MG mode (**a**) and from MG mode to autonomous mode (**b**).

Figures 9 and 10 show the main parameters variation when the IG system is connected/disconnected to/from the inverter-based MG (Figure 9) and how the entire system behaves when, with the IG system operating in parallel with the MG, a significant load is being switched ON and OFF (Figure 10). The data acquisition was set to begin when the transitory process (synchronization, load variation) occurs. Thus, in both the above-mentioned figures the moment of the transitory phenomenon is $t = 0$ s.

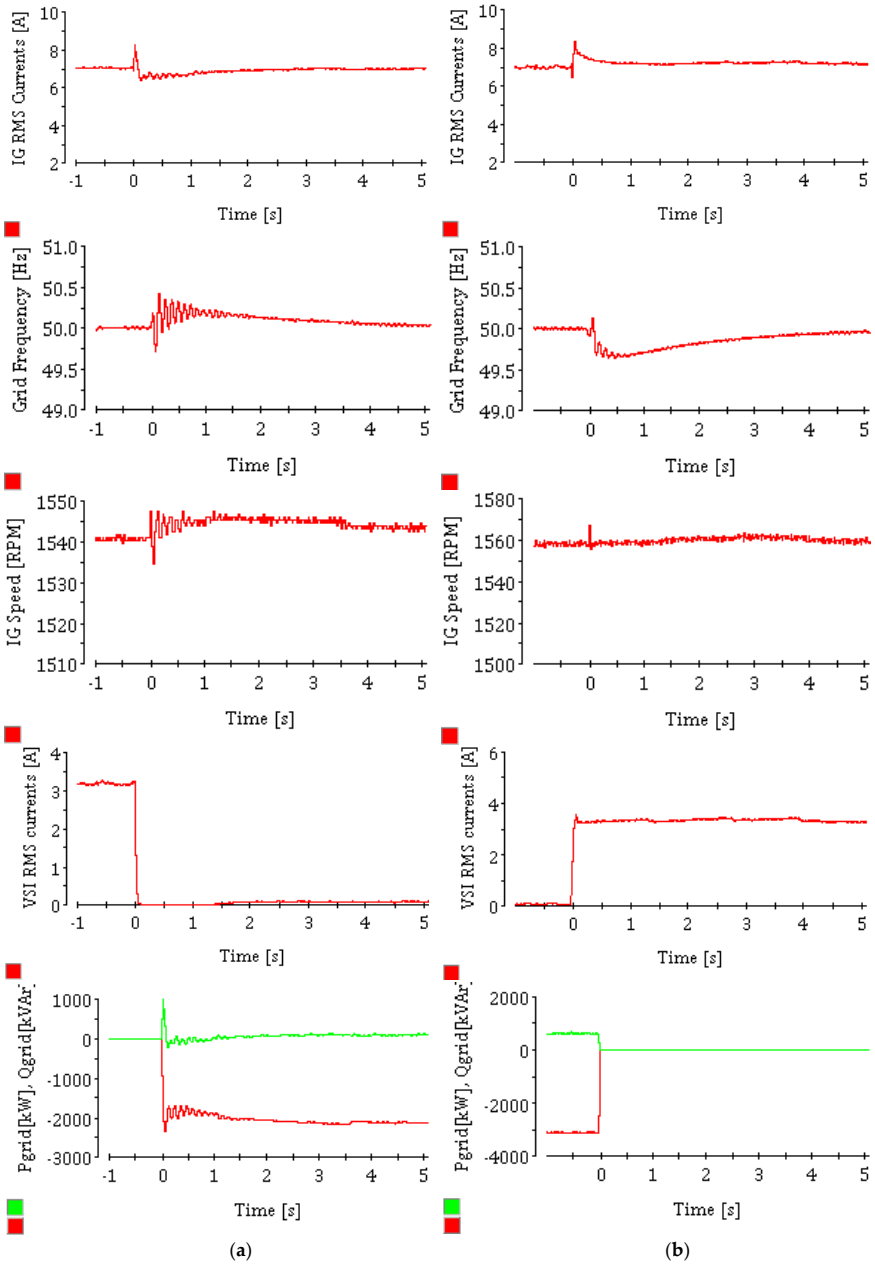

Figure 9. Experimental results for case 1: (**a**) IG system connection to the MG and (**b**) IG system disconnection from the MG.

In the experiments, before the synchronization, the IG was delivering 2 kW and had a very small local load; this particular situation was chosen as the most difficult scenario because it involved the maximum power transfer between the IG system and the MG. The influence of the synchronization process on the IG parameters is shown in Figure 9a. It can be noticed that the IG frequency has a small oscillation right after the K_G relay is closed; it lasts for about 5 s, but within this interval, the frequency value does not exceed the ±50 mHz band around f_0 = 50 Hz imposed by the quality standards. Right after the MG connection, the control of the VSI is disabled, and it will be re-initialized when the MG voltage signal is lost (e.g., during a fault occurring in the MG) and the IG islanded operation is triggered. Thus, the VSI current drops to almost zero, with only a small current circulating through the filter capacitor (C_f). The entire IG active power (P_{grid}) of around 2 kW flows towards the MG; a small amount of reactive power (Q_{grid}) will be drawn from the MG to supplement the one given by the capacitor bank C_{exc}.

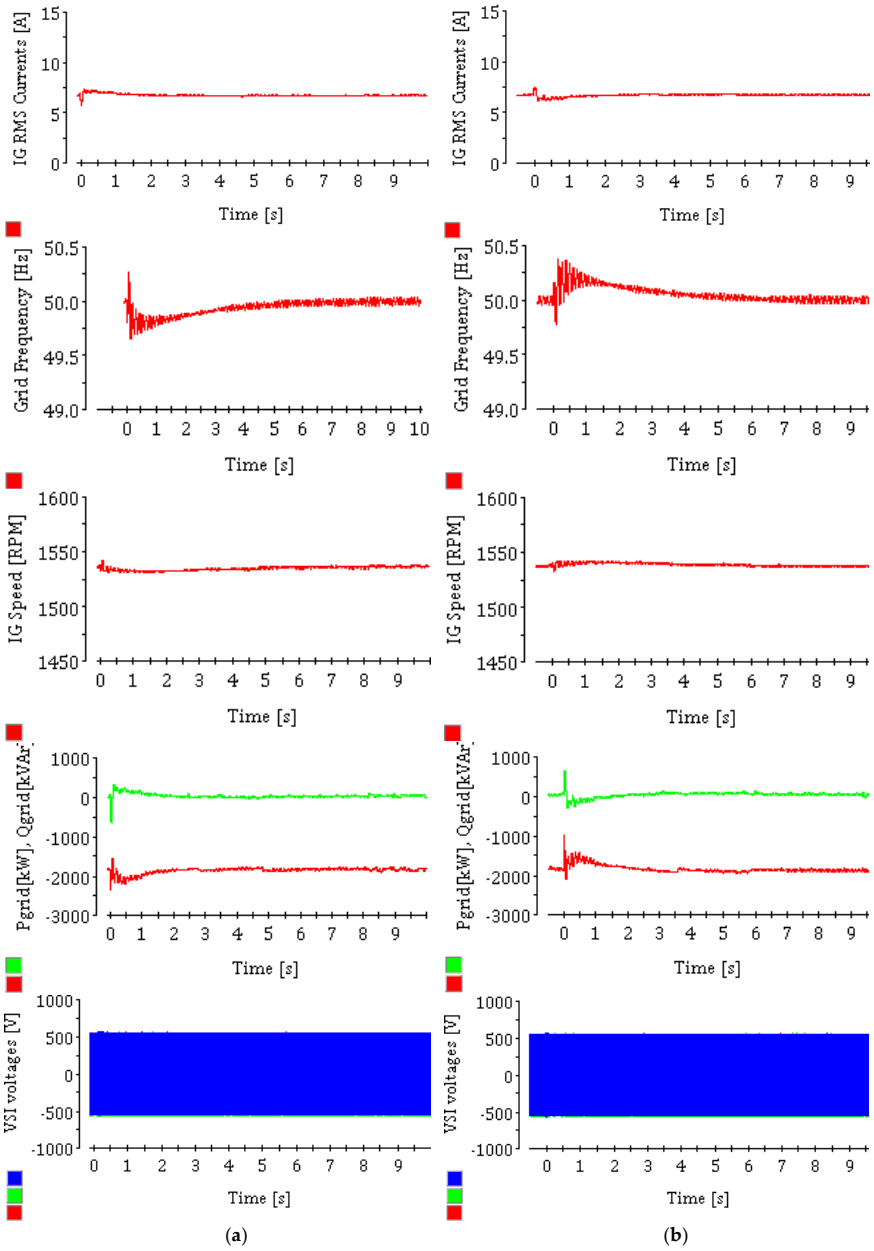

Figure 10. Experimental results for case 2: (**a**) MG load increase and (**b**) MG load decrease.

The IG system disconnection from the MG is also investigated, the K_G switch being manually opened to replicate a real situation in which the MG connection is no longer available. As the IG control system automatically re-initializes the VSI control, a smooth transition into autonomous mode is enabled, as revealed by the waveforms form Figure 9b. The IG system parameters from Table 1 vary in a similar manner for both connection/disconnection processes. More precisely, for the transition to autonomous mode the IG system voltage deviation is 5.73%, while the other three targeted parameters show smaller oscillations compared to the connection process, as the frequency deviation is 0.5%, the IG speed variation 0.27% and the IG active power variation 16.2%.

Next, the behaviour of the IG system operating in parallel with the MG was investigated, for a 2 kW load switching. The relevant experimental results are concentrated in Figure 10. It can be noticed that for both investigates transients, the parameters variations remain within tight limits and do not affect the system stability (in terms of voltage and frequency variations). For example, for MG load increase, the MG frequency (and implicitly the IG speed) deviates no more than 0.7% from the nominal value of 50Hz (i.e., 0.35 Hz), being in good agreement with the results obtained through the

preliminary analysis and shown in Figure 4a. The same pattern is followed by the IG active power deviation, which registers an 18% deviation (i.e., 360 W). The MG voltage deviations are also under 4% from the nominal value.

Thus, as a preliminary conclusion, it can be pointed out that the operation of an IG on an inverter-based MG proves to be beneficial for both the MG and the IG local loads. By means of the built-in VSI, several improvements are under investigation to enhance the IG system with functionalities to further supporting the MG power quality.

Compared with similar topologies, the main advantages of the proposed control structure are as follows:

- Much simpler control: compared with Reference [21], the generation of the control signals for both VSI and DL implies less computational steps/blocks;
- In the case of on-grid to off-grid transition, the voltage variation is 5.73%, compared to 17% in [18], 13.4% in [19] and 16.25% in [21];
- Also, in the case of islanding, the IG speed variation is 0.27%, significantly smaller compared with 15% in Reference [21]—also the IG speed stabilizing time is much smaller in the current paper.

Another aspect worth being mentioned is that overall, the proposed solution provides a high-performance seamless paralleling with the MG and, if the situation requires, an efficient sectionalisation for enhanced local loads supply, rather than to improve significantly the performance of the inverter-based MG. In order to increase the IG support during MG connection, a solution where the VSI is controlled to boost the natural response of the IG is under investigation, aspect which is reserved for future publication.

Finally, it is important to underline that the main goal of the investigated topology was to enable the smooth interconnection of an autonomous IG system with a relatively similar size microgrid, as the literature lacks such solutions. Being simple yet efficient, the proposed control method can be easily scaled to higher power levels. Furthermore, a practical situation that is targeted for the proposed solution is the one in which an autonomous micro-hydro system based on IG is connected in parallel with a PV-based MG with low inertia.

5. Conclusions

A control strategy for an autonomous induction generator (IG) system synchronization and seamless transfer to an inverter-based microgrid (MG) was presented in the current paper. The IG system control in autonomous mode is performed by a combination between a Voltage Source Inverter (VSI) and a Dump Load (DL). The MG consists in an MG leading inverter having on its DC side a supercapacitor-based energy storage system, two MG supporting inverters, and local loads. To ensure a smooth synchronization of the IG system to the inverter-based MG, the VSI control has been enhanced with a synchronisation algorithm. Experimental validations have been accomplished on a complex laboratory test-bench, focusing on the dynamic events associated with the IG system connection/disconnection to/from the MG and also on the MG response to a load being turned on and off when the IG operates connected to the MG. The obtained results showed that the proposed synchronization algorithm ensures a seamless transfer for the IG system from autonomous to MG connected mode and vice-versa. The transfer has been accomplished with affecting neither the IG local load supply nor the MG. Moreover, when a significant load transient occurs within the MG operation and the frequency varies, the IG presence does not influence the MG stability, but rather the contrary, as revealed by the analysis provided in this paper. Based on the findings from this study, further improvements of the IG system to provide more MG-supporting services are considered for future research.

Author Contributions: C.P.I. prepared the literature studies, developed the control of the IG system, analysed the results and wrote the paper. I.S. developed the MG control, performed the analysis from Section 3, conducted the experiments and revised the paper.

Acknowledgments: The work of Serban Ioan was supported by a grant of the Romanian National Authority for Research and Innovation, CCCDI UEFISCDI, project number ERANET LAC Call ELAC2015/T10-0761, RETRACT, within PNCDI III.

Conflicts of Interest: The authors declare no conflict of interest.

Abbreviations

MG	Microgrid
DG	Distributed generator
PLL	Phase locked loop
MGLI	Microgrid leading inverter
MGSI	Microgrid supporting inverter
ESS	Energy storage systems
VSG	Virtual synchronous generator
MHT	Micro hydro turbine
IG	Induction generator
VSI	Voltage source inverter
DL	Dump load
PCC	Point of common coupling

Nomenclature

$V_{DC}{}^*$	DC voltage reference signal
V_{DC}	DC voltage
sn_{IG}, cs_{IG}	sine and cosine of the IG system voltage
sn_G, cs_G	sine and cosine of the grid voltage
f_G	MG frequency
f_{sinc}	synchronisation frequency
ω_{VSG}	VSG speed
H_{VSG}	VSG virtual inertia
T_{mVSG}	virtual mechanical torque
T_{eVSG}	virtual electrical torque
D	damping coefficient
P^*	reference power of the inverter
$\Delta\omega_g$	MG frequency deviation
$\delta\omega_{g2}$	frequency correction signal
K_{fs}	droop response gain
K_{fd}	inertial response gain
s	IG slip
T_{ek}	IG breakdown torque
s_k	IG critical slip
ω_g	MG angular frequency
ω_r	IG rotor angular speed
P	IG pole pairs
T_{m0}	MHT starting torque
K_{MHT}	natural torque-speed control gain of the MHT
J_r	combined generator and MHT inertia coefficient
ΔV	voltage deviation
Δf	frequency deviation
Δn	IG speeddeviation
ΔP_{IG}	IG active power deviation
n_{IG}	IG speed at 2 kW loading
P_{IG}	IG active power
V_{VSI}	VSI output voltage
V_{grid}	MG voltage

Appendix A MG Parameters

		Parameters	Values
Hardware	**IG**	Rated (output) power	3.1 kW
		Nominal voltage	400 V
		Nominal current	8.64 A
		Pole pairs number	2
		Connection type	Delta
	VSI	Rated power	9 kVA
		Output current (continuous)	13 A
		Maximum current	20.8 A
		PWM switching frequency	10 kHz
	Filter	Inductance	3.1 mH
		Capacitance(star-connected)	10 µF
	DC Link	Capacitance	2610 µF
	DL	Average power	2.2 kW
	C_{exc}	Nominal power	7.5 kvar
	MG	Rated power	15 kW
		Rated voltage	400 V
		Rated frequency	50 Hz
Control	**DL regulators**	Proportional gain of PI_1	3
		Integral gain of PI_1	10
		Proportional gain of PI_2	10
		Integral gain of PI_2	30
	VSI regulator	Proportional gain of PI_3	0.15
		Integral gain of PI_3	0.4
	Synchronization regulator	Proportional gain of PI_4	0.03
		Integral gain of PI_4	0.05

References

1. Li, Y.; Yang, Z.; Li, G.; Zhao, D.; Tian, W. Optimal Scheduling of an Isolated Microgrid With Battery Storage Considering Load and Renewable Generation Uncertainties. *IEEE Trans. Ind. Electron.* **2019**, *66*, 1565–1575. [CrossRef]
2. Jin, P.; Li, Y.; Li, G.; Chen, Z.; Zhai, X. Optimized hierarchical power oscillations control for distributed generation under unbalanced conditions. *Appl. Energy* **2017**, *194*, 343–352. [CrossRef]
3. Jaalam, N.; Rahim, N.A.; Bakar, A.H.A.; Tan, C.K.; Haidar, A.M.A. A comprehensive review of synchronization methods for grid-connected converters of renewable energy source. *Renew. Sustain. Energy Rev.* **2016**, *59*, 1471–1481. [CrossRef]
4. Amin, M.R.; Zulkifli, S.A. A framework for selection of grid-inverter synchronisation unit: Harmonics, phase-angle and frequency. *Renew. Sustain. Energy Rev.* **2017**, *78*, 210–219. [CrossRef]
5. Tang, F.; Guerrero, J.M.; Vasquez, J.C.; Wu, D.; Meng, L. Distributed Active Synchronization Strategy for Microgrid Seamless Reconnection to the Grid Under Unbalance and Harmonic Distortion. *IEEE Trans. Smart Grid* **2015**, *6*, 2757–2769. [CrossRef]
6. Abhinav, S.; Schizas, I.D.; Ferrese, F.; Davoudi, A. Optimization-Based AC Microgrid Synchronization. *IEEE Trans. Ind. Inform.* **2017**, *13*, 2339–2349. [CrossRef]
7. Sun, Y.; Zhong, C.; Hou, X.; Yang, J.; Guerrero, J.M. Distributed cooperative synchronization strategy for multi-bus microgrids. *Int. J. Electr. Power Energy Syst.* **2017**, *86*, 18–28. [CrossRef]

8. Wang, C.; Liang, B.; He, J. An Enhanced Power Regulation and Seamless Operation Mode Transfer Control Through Cooperative Dual-Interfacing Converters. *IEEE Trans. Smart Grid* **2018**, *9*, 5576–5587. [CrossRef]
9. Wai, R.-J.; Lin, C.-Y.; Huang, Y.-C.; Chang, Y.-R. Design of High-Performance Stand-Alone and Grid-Connected Inverter for Distributed Generation Applications. *IEEE Trans. Ind. Electron.* **2013**, *60*, 1542–1555. [CrossRef]
10. Shah, D.S.; Sun, H.; Nikovski, D.; Zhang, J. VSC-Based Active Synchronizer for Generators. *IEEE Trans. Energy Convers.* **2018**, *33*, 116–125. [CrossRef]
11. Hassan, M.A. Dynamic Stability of an Autonomous Microgrid Considering Active Load Impact With a New Dedicated Synchronization Scheme. *IEEE Trans. Power Syst.* **2018**, *33*, 4994–5005. [CrossRef]
12. Sekhar, V.C.; Kant, K.; Singh, B. DSTATCOM supported induction generator for improving power quality. *IET Renew. Power Gener.* **2016**, *19*, 495–503. [CrossRef]
13. Chauhan, P.J.; Chatterjee, J.K. A Novel Speed Adaptive Stator Current Compensator for Voltage and Frequency Control of Standalone SEIG Feeding Three-Phase Four-Wire System. *IEEE Trans. Sustain. Energy* **2019**, *10*, 248–256. [CrossRef]
14. Danang Wijaya, F.; Firmansyah, E.; Sarjiya; Isnaeni, B.S.M. Grid connected-induction generator start-up sequence observation using laboratory simulator. In Proceedings of the 2015 IEEE Innovative Smart Grid Technologies—Asia (ISGT ASIA), Bangkok, Thailand, 3–6 November 2015; pp. 1–5.
15. Gorski, D.A.; Balkowiec, T.; Koczara, W. Grid Connection of a Converter Controlled Squirrel-Cage Induction Generator. In Proceedings of the 2018 7th International Conference on Renewable Energy Research and Applications (ICRERA), Paris, France, 14–17 October 2018; pp. 348–353.
16. Tunyasrirut, S.; Wangsilabatra, B.; Suksri, T. Phase control thyristor based soft-starter for a grid connected induction generator for wind turbine system. In Proceedings of the ICCAS 2010, Gyeonggi-do, South Korea, 27–30 October 2010; pp. 529–534.
17. Arthishri, K.; Kumaresan, N.; Ammasaigounden, N. Analysis and MPPT control of a wind-driven three-phase induction generator feeding single-phase utility grid. *J. Eng.* **2017**, *6*, 220–231. [CrossRef]
18. Cagnano, A.; De Tuglie, E.; Cicognani, L. Prince—Electrical Energy Systems Lab A pilot project for smart microgrids. *Electr. Power Syst. Res.* **2017**, *148*, 10–17. [CrossRef]
19. Cagnano, A.; De Tuglie, E.; Trovato, M.; Cicognani, L.; Vona, V. A simple circuit model for the islanding transition of microgrids. In Proceedings of the 2016 IEEE 2nd International Forum on Research and Technologies for Society and Industry Leveraging a Better Tomorrow (RTSI), Bologna, Italy, 7–9 September 2016; pp. 1–6.
20. Singh, B.; Pathak, G.; Panigrahi, B.K. Seamless Transfer of Renewable-Based Microgrid Between Utility Grid and Diesel Generator. *IEEE Trans. Power Electron.* **2018**, *33*, 8427–8437. [CrossRef]
21. Chen, W.-L.; Xie, C.-Z. Active Voltage and Frequency Regulator Design for a Wind-Driven Induction Generator to Alleviate Transient Impacts on Power Grid. *IEEE Trans. Ind. Electron.* **2013**, *60*, 3165–3175. [CrossRef]
22. Serban, I. A control strategy for microgrids: Seamless transfer based on a leading inverter with supercapacitor energy storage system. *Appl. Energy* **2018**, *221*, 490–507. [CrossRef]
23. Serban, I.; Ion, C.P. Microgrid control based on a grid-forming inverter operating as virtual synchronous generator with enhanced dynamic response capability. *Int. J. Electr. Power Energy Syst.* **2017**, *89*, 94–105. [CrossRef]
24. Wang, Z.; Wang, J. Self-healing resilient distribution systems based on sectionalization into microgrids. *IEEE Trans. Power Syst.* **2015**, *30*, 3139–3149. [CrossRef]
25. Chowdhury, S.; Chowdhury, S.P.; Crossley, P. *Microgrids and Active Distribution Networks*; Institution of Engineering and Technology: London, UK, 2009; ISBN 978-1-84919-014-5.
26. Ion, C.P.; Marinescu, C. Autonomous micro hydro power plant with induction generator. *Renew. Energy* **2011**, *36*, 2259–2267. [CrossRef]
27. Ion, C.P.; Serban, I. Self-Excited Induction Generator Based Microgrid with Supercapacitor Energy Storage to Support the Start-up of Dynamic Loads. *Adv. Electr. Comput. Eng.* **2018**, *18*, 51–60. [CrossRef]

28. Serban, I.; Marinescu, C. Control Strategy of Three-Phase Battery Energy Storage Systems for Frequency Support in Microgrids and with Uninterrupted Supply of Local Loads. *IEEE Trans. Power Electron.* **2014**, *29*, 5010–5020. [CrossRef]
29. Boldea, I.; Nasar, S.A. *The Induction Machine Design Handbook*, 2nd ed.; CRC Press: Boca Raton, FL, USA, 2010; ISBN 978-1420066685.